Electromagnetic backscattering from freak waves in (1+1)-dimensional deep-water*

Xie Tao(谢 涛)[a)b)†], Shen Tao(沈 涛)[a)], William Perrie[b)], Chen Wei(陈 伟)[a)], and Kuang Hai-Lan(旷海兰)[a)]

[a)] *School of Information Engineering of Wuhan University of Technology, Wuhan* 430070*, China*
[b)] *Bedford Institute of Oceanography, B2Y 4A2, Dartmouth, NS, Canada*

(Received 21 August 2009; revised manuscript received 11 October 2009)

To study the electromagnetic (EM) backscatter characteristics of freak waves at moderate incidence angles, we establish an EM backscattering model for freak waves in (1+1)-dimensional deep water. The nonlinear interaction between freak waves and Bragg short waves is considered to be the basic hydrodynamic spectra modulation mechanism in the model. Numerical results suggest that the EM backscattering intensities of freak waves are less than those from the background sea surface at moderate incidence angles. The normalised radar cross sections (NRCSs) from freak waves are highly polarisation dependent, even at low incidence angles, which is different from the situation for normal sea waves; moreover, the NRCS of freak waves is more polarisation dependent than the background sea surface. NRCS discrepancies between freak waves and the background sea surface with using horizontal transmitting horizomtal (HH) polarisation are larger than those using vertical transmitting vertical (VV) polarisation, at moderate incident angles. NRCS discrepancies between freak waves and background sea surface decreases with the increase of incidence angle, in both HH and VV polarisation radars. As an application, in the synthetic-aperture radar (SAR) imaging of freak waves, we suggest that freak waves should have extremely low backscatter NRCSs for the freak wave facet with the strongest slope. Compared with the background sea surface, the freak waves should be darker in HH polarisation echo images than in VV echo images, in SAR images. Freak waves can be more easily detected from the background sea surface in HH polarisation images than in VV polarisation images. The possibility of detection of freak waves at low incidence angles is much higher than at high incidence angles.

Keywords: freak wave, nonlinearities, electromagnetic backscattering, sea surface
PACC: 4120, 4110H

1. Introduction

Freak waves have become an active research topic in engineering and science over the past 20 years. The notion of freak waves was first introduced by Draper.[1] According to the Rayleigh distribution of wave heights, a freak wave is an extremely unlikely wave whose height exceeds 2.2 times the significant wave height H_s of the background sea.[2,3] The study of freak waves started in the late 1980's. How high is the highest freak wave? What properties does it have? How often and under what circumstances does the extreme wave occur? These and additional questions have been studied.[4−17]

Freak waves have been observed in both shallow and deep water, with and without the presence of strong currents. Many explanations and possible mechanisms have been proposed to analyse their formation subject to the specific physical conditions. Why do freak wave phenomena occur? There are many possible reasons. Generally, in shallow water areas, extreme wave events can be explained by the presence of ocean currents or bottom topography that may cause wave energy to focus in a small area because of refraction, reflection, and wave trapping. These mechanisms may be explained by linear wave theory.[18] The nonlinear effects on freak waves are discussed by Yasuda *et al.*[19,20] They drew a conclusion that third order nonlinear interactions enhance the occurrence of freak waves and are the primary cause of freak wave generation in a general wave field except for the case of strong wave-current interactions or wave diffraction behind an island. In areas where waves from storms in the open ocean approach shallower waters, the waves

*Project supported by the National High Technology Research and Development Program of China (Grant No. 2007AA12Z170), the National Natural Science Foundation of China (Grant No. 40706058), the Science-Technology Chenguang Foundation for Young Scientist of Wuhan, China (Grant No. 200850731388) and the Wind and Waves Component of the Canadian Space Agency GRIP Project Entitled Building Satellite Data into Fisheries and Oceans Operational Systems.
†Corresponding author. E-mail: xtplqk@whut.edu.cn
© 2010 Chinese Physical Society and IOP Publishing Ltd

will be refracted and diffracted. Fedele and Arena[21] extend the quasi-deterministic theory of Boccotti[22,23] to the second-order case, deriving new wave crest and wave trough distributions that take into account nonlinear effects and hold true for the finite bandwidth of the spectrum in deep-water.

Several numerical studies give results for freak waves in deep water.[15,24,25] Schober,[25] Islas and Schober[26] investigated freak waves within the framework of the nonlinear Schördinger (NLS) equation and related the development of freak waves in oceanic sea states characterised by the Joint North Sea Wave Project (JONSWAP) spectral with the proximity to homoclinic solutions of the NLS equation. Using the inverse spectral theory of the NLS equation, they built a model for predicting freak waves in deep water. Osborne *et al.*[24] discussed analytical results for 1+1 dimensions (i.e. spatial dimension and temporal dimension) and demonstrated numerically, for certain sets of initial conditions, the ubiquitous occurrence of freak waves in 2+1 dimensions (2 spatial dimensions and 1 temporal dimension). They obtained a conclusion that a typical wave field evidently consists of a background of stable wave modes punctuated by the intermittent up-thrusting of unstable rogue waves.

Recently, for the purpose of the detection of freak wave events, Lehner *et al.*[27,28] analysed synthetic-aperture radar (SAR) wave mode images from the Environmental Research Satellite (ERS) and ENVISAT satellites, and found the wellknown Draupner time series, in which a wave of 26 m in height was measured. They also found high wave groups in the case where storm systems move at the group speed of the ocean waves. In order to detect freak wave targets on or above the storm sea surface by radar, the electromagnetic (EM) backscattering characteristics of freak waves must be studied. The EM wave backscatter results from a rough sea surface and has been studied by many different methods in recent years, such as Kirchhoff approximation (KA), physical optics (PO), small perturbation approximation (SPA) and Bragg scattering (see, for example, Refs. [29]–[44]. In the present paper, our intention is to numerically analyse the EM backscattering characteristics of freak waves in 1+1 dimensions in deep-water. As far as we know, this topic has received little attention thus far.

A freak wave model is presented in Section 2, and a two-scale freak wave sea surface model is given in Section 3. In Section 4, an EM Backscattering model of the two-scale freak wave sea surface is presented. We also give the numerical results and discussion.

2. Long freak wave in (1+1)-dimensional deep sea

Here we use the freak wave model in (1+1)-dimensional deep sea presented by Osborne *et al.*[24] Because it is an analytical solution to describe freak waves, one can easily use it to calculate EM backscattering intensity from freak wave. In the (1+1)-dimensional deep sea, the envelop soliton or the breathers solutions of the NSL equation are related to the freak wave sea surface.[24,45,46] Osborne *et al.*[24] gave two analytical examples of unstable modes which are readily found from the periodic inverse scattering transform (IST) solution for the (1+1)-dimensional NLS equation in the 1-dimensional form. Here we rewrite the NLS equation given by Osborne *et al.* as follows:[24]

$$\mathrm{i}u_T + u_{XX} + 2\left|u\right|^2 u = 0. \tag{1}$$

Equation (1) turns back to the equation given by Osborne *et al.*[24] by using $u = \lambda\psi$, $X = x - C_g t$, $T = \mu t$, and $\lambda = \sqrt{\nu/2\mu}$, where $C_g = \omega_0/2k_0$, $\mu = \omega_0/8k_0^2$ and $\nu = \omega_0 k_0^2/2$, where k_0 is the carrier wave number and ω_0 is its frequency, the dispersion relation is $\omega_0 = \sqrt{gk_0}$ and g is the acceleration of gravity. For the purpose of simulating a freak wave sea surface, following the way of Osborne *et al.*,[24] we select particular homoclinic solutions of Eq. (1), i.e. for $\lambda = \mathrm{i}a/\sqrt{2}$,

$$\begin{aligned} & A_{\mathrm{f}}(x,t) \\ = & -\mathrm{i}\sqrt{2}\,\mathrm{e}^{2\mathrm{i}a^2T} \\ & \times \left[\frac{\cos[\sqrt{2}aX]\,\mathrm{sech}[\sqrt{2}a^2T] + \mathrm{i}\sqrt{2}\tanh\left[2a^2T\right]}{\sqrt{2} - \cos[\sqrt{2}aX]\,\mathrm{sech}[\sqrt{2}a^2T]}\right], \end{aligned} \tag{2}$$

where $A_{\mathrm{f}}(x,t)$ denotes the complex envelope function of a deep-water wave train whose surface elevation is

$$\xi_{\mathrm{f}}(x,t) = \mathrm{Re}\left[A_{\mathrm{f}}(x,t)\,\mathrm{e}^{\mathrm{i}(k_0x - \omega_0 t)}\right], \tag{3}$$

where $a > 0$ is an initial regular envelop amplitude. Thereafter the elevation of the freak wave surface in the (1 + 1)-dimensional deep sea is

$$\xi_{\mathrm{f}} = B(x,t)/C(x,t), \tag{4}$$

where

$$\begin{aligned} B(x,t) = & \ 2\tanh(2a^2T)\cos(\psi_0) + \sqrt{2}\cos(\sqrt{2}aX) \\ & \times \ \mathrm{sech}(\sqrt{2}a^2T)\sin(\psi_0), \end{aligned}$$

$$C(x,t) = \sqrt{2} - \cos(\sqrt{2}aX)\,\mathrm{sech}(\sqrt{2}a^2T),$$

and

$$\psi_0 = k_0 x - \omega_0 t + 2a^2 T.$$

Following Eqs. (2) and (4), we simulate the freak sea surface as shown in Fig. 1. From Fig. 1, one can find that the maximum height is more than $2.2H_{\mathrm{s}}$, where H_{s} is the significant wave height of the group. Thus, we can simulate the long-scale freak wave sea surface with the selected model.

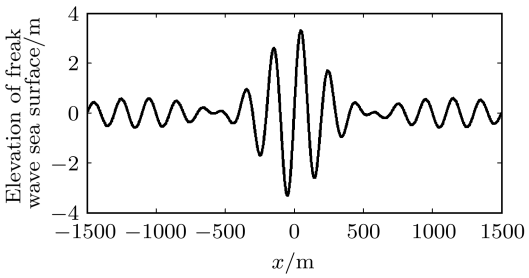


Fig. 1. Spatial evolution of a freak wave sea surface in the deep sea, where wavelength $\lambda = 200$ m, -1500 m$\leq x \leq$ 1500 m at time $t = 0$.

3. Two-scale freak wave sea surface model

The incident electromagnetic wave is scattered by the sea surface. The main EM scattering mechanism is Bragg scattering for small scale waves. The normalised radar corss section (NRCS) is modulated (which is called tilt modulation) by the long waves. To calculate multiple polarized NRCS for freak waves, we use a similar method to that given by Franceschetti *et al.*[44] except that we only consider one spatial dimension.

3.1. Facets of long freak waves

Long waves (or freak waves) can be modeled by Eq. (4). They can be divided into a number of scattering facets by using the criterion (according to Franceschetti *et al.*[44]):

$$L_x = \frac{\lambda_e}{8\,|s'_x - s_x|\cos\theta}\,, \tag{5}$$

where θ is the incidence angle of the EM wave, λ_e is the EM wavelength, L_x is the length of facet, s'_x and s_x (equation (8)) are the slope of a given facet and that of the next neighboring facet, respectively. For each facet, one can select the same value of $|s'_x - s_x|$.

3.2. Bragg short waves riding on freak waves

According to the Bragg scattering mechanism of small scale Bragg waves whose wave-numbers satisfy

$$k_b(\theta) = 2k_e \sin\theta. \tag{6}$$

For each facet, there is a different Bragg short wave. There are N backscattering facets within a certain SAR image pixels. On the nth facet, the relative elevation of this facet is

$$\xi_r(x,t,\theta)|_{x=x_n} = \xi_b(x,t,\theta) + s_x L_x|_{x=x_n}\,, \tag{7}$$

where s_x is the slope of this facet, and

$$s_x|_{x=x_n} = \xi_x|_{x=x_n} = \frac{\partial}{\partial x}\xi_{\mathrm{f}}(x,t)\bigg|_{x=x_n}\,, \tag{8}$$

where $\xi_x = \mathrm{d}\xi_{\mathrm{f}}(x,t)/\mathrm{d}x$ can be calculated following the appendix of Ref. [47]. Moreover, $\xi_b(x,t,\theta)$ should satisfy

$$\xi_b(x,t,\theta) = a_b(\theta)\sin(\psi_b(\theta)), \tag{9}$$

where

$$\psi_b(\theta) = k_b(\theta)x - \omega_b(\theta)t + \varphi_b(\theta), \tag{10}$$

$$\omega_b(\theta) = \sqrt{g k_b(\theta)}, \tag{11}$$

$$a_b(\theta) = a_{bb}\sqrt{\frac{S(k_b(\theta))}{S(k_{bb})}}, \tag{12}$$

where $S(k_b(\theta))$ and $S(k_{bb})$ denote the spectrum intensity of the Bragg wave and that of another short wave with a different wave number, respectively.

The short wave spectrum $S(k)$ is truncated from the 1D Pierson–Moskowitz (PM) spectrum:[48]

$$S(k) = \frac{\alpha}{4k^3}\exp\left(-\frac{0.74g^2}{k^2 W S P_{19.5}^4}\right), \tag{13}$$

where $\alpha = 0.0081$, and $\mathrm{WSP}_{19.5}$ is the wind speed at 19.5 m above sea surface.

Thus, from Subsections 3.1 and 3.2, one can obtain a two-scale freak sea surface model whose elevation is

$$\xi(x,t,\theta) = \xi_{\mathrm{f}}(x,t,\theta) + \xi_r(x,t,\theta). \tag{14}$$

4. Backscatter from a freak wave sea surface

We consider multiple polarised backscatter from a freak wave sea surface. The polarisations include vertical transmitting-vertical receiving EM wave (VV polarisation), horizontal transmitting-horizontal receiving EM wave (HH), vertical transmitting-horizontal

receiving EM wave (VH polarisation) and horizontal transmitting-vertical receiving EM wave (HV polarisation). But for our case, i.e. VH and HV polarisations, the EM backscattering intensities are zero, owing to the Bragg scattering mechanism.

Before creating an EM backscattering model for the freak sea surface, we discuss the two main NRCS modulations related to long freak waves.

4.1. NRCS tilt modulation by long freak wave

As mentioned above, we consider the Bragg scattering mechanism for EM scattering from ripples. The Bragg backscattering NRCS is modulated by tilt modulation of long freak waves. For the nth facet, its gravity point is denoted by $P_n(x_n, \xi_{\mathrm{f}(n)})$ and its slope is represented by s_{x_n}. For each facet, the incident angle θ in Eq. (6) is determined by the local incidence angle. Let the local incident angle be θ_{local}, which is related to the local normal, then we will have

$$\theta_{\mathrm{local}} = \begin{cases} \theta + \tan^{-1} s_x, & \tan^{-1} s_x < 90^\circ, \\ \left|\theta + \tan^{-1} s_x - 180^\circ\right|, & \tan^{-1} s_x \geq 90^\circ. \end{cases} \tag{15}$$

Using Eqs. (9)–(14), one can create a model which includes Bragg scattering from ripples in facets and tilt modulation of the NRCS by long freak waves. In fact, because we estimate maximum value of $\tan^{-1}\mathrm{s}_x$ to be about 6° and the minimum value of $\tan^{-1}\mathrm{s}_x$ to be about 175°, we can ensure that the Bragg scattering condition is satisfied in our study by restricting θ_{local} to be within a range from 20° to 84° (The range from 20° to 84° is the incidence angle limitation of two-scale Bragg EM backscattering model) when θ is restricted within (26°, 79°).

4.2. NRCS hydrodynamic modulation by long freak waves

A second important NRCS modulation is the Bragg wave spectrum nonlinear hydrodynamics modulation by long freak waves.

For the incidence angle of each EM wave, the corresponding Bragg short wave number can be determined by $k_b(\theta) = 2k_e \sin\theta$. The Bragg short wave amplitude $a_b(\theta)$ can be calculated from Eq. (12) if there are no nonlinear interactions (i.e. hydrodynamic modulation) between Bragg waves and long freak waves. Unfortunately, the hydrodynamic modulation of short waves by long waves should not be ignored (see Ref. [49]). Thus, hydrodynamic modulation needs to be considered when one determines the Bragg parameters.

According to Ref. [49], wave-number and amplitude expressions of short Bragg waves that are modulated by long freak waves can be written as follows:

$$k_b(x,t,\theta) = k_{bb}\left(1 + |A_{\mathrm{f}}|\, k_{\mathrm{f}} \sin\psi_{\mathrm{f}}\right), \tag{16}$$

$$a_b(x,t,\theta) = a_{bb}\left(1 + |A_{\mathrm{f}}|\, k_{\mathrm{f}} \sin\psi_{\mathrm{f}}\right), \tag{17}$$

where k_{bb} is the wave number of short wave which would be modulated by long freak waves and a_{bb} is its amplitude, subscript f refers to the freak wave.

From Eqs. (16) and (17), one can find that the Bragg wave number, amplitude and phase vary with those of the freak wave at different spatial sites and temporal points. This means we have to calculate those parameters for each facet. Our main purpose in this section is to determine $a_b(x,t,\theta)$ which is used to feedback to Eq. (9).

To solve $a_b(x,t,\theta)$ from Eq. (17), a_{bb}, $|A_{\mathrm{f}}|$, k_{f} and ψ_{f} (includes ω_{f}, φ_{f}) should be evaluated, while a_{bb} can be derived from Eq. (16). Thus, first of all, one should compute the parameters of the freak wave according to Refs. [47] and [50]. One can obtain $|A_{\mathrm{f}}|$ from Eq. (2). We present a new method to derive k_{f}, ω_{f} and φ_{f}, here.

Before introducing the numerical method, we present the following concepts.

(i) A given freak wave (whose subscript is f) can be considered as a 'nonlinear long wave' when a short wave (which will be hydrodynamically modulated by the freak wave to become a Bragg short wave—its parameters are denoted by subscript *bb*) rides on the long freak wave.

(ii) Frequencies, amplitudes and wave numbers may be variable. Long freak waves can be regarded as waves whose frequencies, amplitudes and wave numbers vary temporally and spatially.

(iii) A given long freak wave can be considered to be discrete; there is a corresponding amplitude and wave number at every temporal and spatial point. The surface elevation of the long freak wave at a given location can be regarded as corresponding to the surface elevation of a sine wave whose amplitude and wavenumber are those of the long freak wave at that point.

(iv) Discrete interactions between a long freak wave and short wave are assumed. The result of interactions between a long freak wave and short waves

can be regarded as the sum of interactions between short waves and different sine waves whose amplitude and wave-numbers are equal to those of the long freak wave at different points.

Therefore, Eq. (4) can also be expressed as the set function of all temporal and spatial points (x_i, t_j):

$$\begin{aligned}&\xi_{\rm f}(x_i,t_j)\\ =\ &|A_{\rm f}(x,t)|\sin\psi_{\rm f}|_{(x_i,t_j)}\\ =\ &|A_{\rm f}(x_i,t_j)|\sin(k_{\rm f}(x_i,t_j)x_i\\ &-\omega_{\rm f}(x_i,t_j)t_j+\varphi_{\rm f}(x_i,t_j)),\end{aligned}\tag{18}$$

where i and j are the spatial and temporal indices, respectively, and spatial and temporal variables $\mathrm{a}(x_i, t_j)$ in Eqs. (16) and (17).

According to Ref. [43], one can derive the corresponding wave numbers $k_{\rm f}(x_j, t_k)$, frequencies $\omega_{\rm f}(x_j, t_k)$ and initial phases $\varphi_{\rm f}(x_j, t_k)$. Substituting $k_{\rm f}(x_j, t_k)$, $\omega_{\rm f}(x_j, t_k)$, $\varphi_{\rm f}(x_j, t_k)$ and Eq. (6) into Eq. (16), one can obtain k_{bb}. With Eq. (12), one can obtain a_{bb} at k_{bb}. Then $a_b(x, t, \theta)$ can be obtained from Eq. (17).

Here we mention that the solved amplitude $a_b(x, t, \theta)$ which corresponds to wave number $k_b(x, t, \theta)$ is only one component of spectra intensity which is transferred from the short wave spectra before it is modulated by freak waves. Thus to obtain the Bragg wave amplitude $a_b(\theta)$ in Eq. (9) at a specific time and location such as (x_i, t_j), we calculate the amplitude distribution $\overline{< a_b(\theta) >}$ (averaged in temporal domain) for the wave number domain corresponding to all incident angles of interest, then we use $\overline{< a_b(\theta) >}$ to replace $a_b(\theta)$ in Eq. (9) for each wave number separately.

4.3. Multiple polarised backscattering coefficients

In the present paper, as the method of solving multiple polarised backscatter coefficients is similar to that given by Franceschetti *et al.*,[44] we briefly introduce the results of our case.

We consider moderate incidence angles $\theta(20^\circ \le \theta \le 84^\circ)$ which are coincide with the incident angles of SAR, and we assume that the EM backscattering is dominated by the Bragg scattering mechanism. The sea surface has an infinite conductibility, and its reflectivity does not change. The shadowing effect and the multiple scattering are neglected.

Let the 2×2 matrix $\boldsymbol{\Gamma}$ denote the multiple polarised backscattering coefficient matrix. The relation between backscattering fields and incident fields is

$$\begin{bmatrix}E_v\\E_h\end{bmatrix}^s=\frac{\mathrm{j}k_e\,\mathrm{e}^{-\mathrm{j}k_eR}}{4\pi R}\Gamma\begin{bmatrix}E_v\\E_h\end{bmatrix}^{\rm i},\tag{19}$$

where R is the distance between receiver and scatter, E_v and E_h are vertical and horizontal polarised components of electric field, respectively, and

$$\begin{aligned}\boldsymbol{\Gamma}\ =\ &\left[\overline{\overline{\boldsymbol{I}}}-\boldsymbol{k}\boldsymbol{k}\right]F\exp(\mathrm{j}2k_e\xi_{x_n}\cos\theta)\\ &\times\int_{L_x}\sqrt{1+\xi_x^2}\exp(\mathrm{j}2\boldsymbol{k}_e\cdot\boldsymbol{r}')\,\mathrm{d}x\\ =\ &\begin{bmatrix}S_{vv}&S_{vh}\\S_{hv}&S_{hh}\end{bmatrix}\cdot\int_{L_x}\sqrt{1+s_x^2}\exp(\mathrm{j}2\boldsymbol{k}_e\cdot\boldsymbol{r}')\,\mathrm{d}x\\ =\ &S\cdot U,\end{aligned}\tag{20}$$

where

$$U=\int_{L_x}\sqrt{1+s_x^2}\exp(\mathrm{j}2\boldsymbol{k}_e\cdot\boldsymbol{r}')\,\mathrm{d}x,\tag{21}$$

$\overline{\overline{\boldsymbol{I}}}$ is the identity matrix, $\boldsymbol{k}_e$ is the incident electromagnetic wave propagation vector, $\boldsymbol{r}'$ is the spatial location vector of the sea surface facet. For backscattering, the VH polarisation coefficient has the same value as that of HV polarisation, i.e., $S_{vh} = S_{hv}$.

The backscattering coefficients are

$$S_{hh}=\frac{-2\cos(\Delta\theta)}{s_x^2+\sin^2(\Delta\theta)}(s_x^2R_q-R_p\sin^2(\Delta\theta)),\tag{22}$$

$$S_{hv}=S_{vh}=\frac{-s_x\sin^2(\Delta\theta)}{s_x^2+\sin^2(\Delta\theta)}(R_p+R_q),\tag{23}$$

$$S_{vv}=\frac{-2\cos(\Delta\theta)}{s_x^2+\sin^2(\Delta\theta)}(R_q\sin^2(\Delta\theta)-s_x^2R_p),\tag{24}$$

where $\Delta\theta = \theta - \theta_0$ is the difference in angle between incidence angle θ and the incidence angle θ_0 in the radar beam centre. R_p and R_q are the Fresnel reflection coefficients and given as

$$R_p=\frac{\cos\theta_l-\sqrt{\varepsilon_r-\sin^2\theta_l}}{\cos\theta_l+\sqrt{\varepsilon_r-\sin^2\theta_l}},\tag{25}$$

$$R_q=\frac{\sqrt{\varepsilon_r-\sin^2\theta_l}-\varepsilon_r\cos\theta_l}{\sqrt{\varepsilon_r-\sin^2\theta_l}+\varepsilon_r\cos\theta_l},\tag{26}$$

where $\cos\theta_l = (s_x\sin\theta+\cos\theta)/\sqrt{1+s_x^2}$, θ_l is local incident angle with respect to the local normal, and $\varepsilon_r = 81.5$ for normal sea water.

Substitute Eqs. (7), (8) and (14) into Eq. (25), one can obtain the discrete form of U

$$U\ =\ \frac{2\pi I}{k_b(\theta)}\sum_{m=0}^{\infty}J_m\left[2a_b(\theta)k_e\cos\theta\right]\cdot\exp[\mathrm{j}m\phi_b(\theta)]$$

$$\times \sin c\left[I\left(\frac{2\pi k_e}{k_b(\theta)}s_x\cos\theta - m\pi\right)\right] \times \cos\left(\frac{2\pi k_e}{k_b(\theta)}s_x\cos\theta - m\pi\right), \quad (27)$$

where I is the Bragg short wave number within the facet, and $J_m(\cdot)$ is a Bessel function series.

5. Numerical results

In this section, we simulate the corresponding NRCS by using the backscattering coefficients. We present not only numerical results of backscattering from a freak sea surface (for the purpose of validating our EM scattering model) but also a comparison of NRCS between a sea surface composed of sine waves and a freak wave.

The NRCS is related to backscattering coefficient by the following expression:

$$\sigma^0 = \frac{1}{X\cos\theta}\left|\boldsymbol{\Gamma}\right|^2, \quad (28)$$

where X is the width of the incident EM wave.

5.1. Validation of EM scattering model

Before calculating the backscattering intensities of freak waves, for the purpose of validation of our EM scattering model, we simulate the NRCS of sine wave with Bragg short waves on it. We then compare this result with accepted knowledge. The amplitude and the wavelength of sine waves are 0.8 m and 200 m, respectively (see Fig. 2). The scattering area extends from –200 to 200 m. The SAR imaging pixel size is 10 m. The RADARSAT2 frequency (5.405×10^9 Hz) is used as a frequency of the incident EM wave. Local wind speed is 10 m/s. The incidence angle is 30°. The NRCSs for sine waves can be computed with our EM scattering model and the above parameters, and they can be shown to vary with x as shown in Fig. 3.

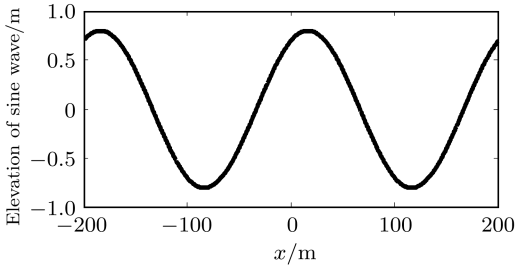


Fig. 2. Elevation of sine wave, whose amplitude is 0.8 m, $\lambda = 200$ m, -200 m$\leq x \leq 200$ m, at $t = 0$.

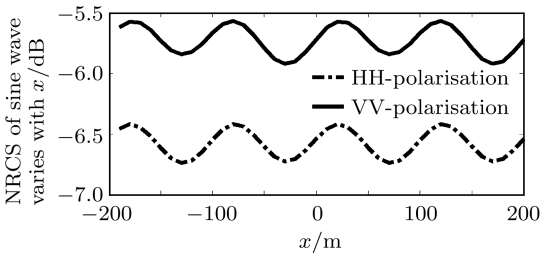


Fig. 3. Variations of NRCSs for sine wave with x for HH and VV polarisations.

From Fig. 3 it follows that the NRCSs of sine waves vary with distance in x direction nearly in a period (0.5 times wave length), the NRCS of VV polarisation is larger than that of in HH polarisation at the same location. This coincides with the results of Franceschetti *et al.*[44] Over a given period, the NRCS is largest at crest and trough in Fig. 2 while is smallest at average sea level.

We average the backscattering NRCS of sine waves within the area of interest (see Fig. 2). The result in Fig. 4 shows that both averaged NRCSs (VV and HH polarisations) of sine waves decrease with the increase of incidence angle. Comparing the averaged NRCS for VV polarisation with the NRCS for HH polarisation, one can find that the polarisation ratio (VV/HH) increases with the increase of incidence angle as shown in Fig. 5. These results coincide with the accepted results (such as those given by Kudryavtsev *et al.*[43]).

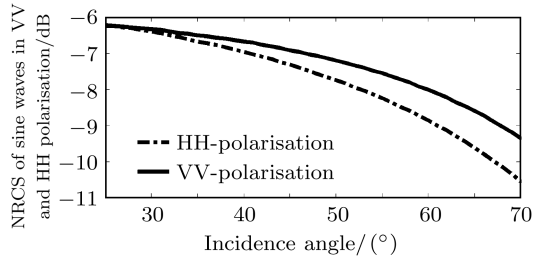


Fig. 4. NRCSs of sine waves, where solid line represents VV polarisation and dash line corresponds to HH polarisation.

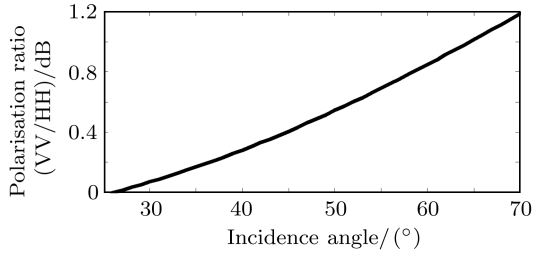


Fig. 5. Polarisation ratio (VV/HH) of sine wave.

Moreover, from our numerical results, backscattering coefficients of different kinds of sea surfaces

(sine wave, background sea surface (environment sea surface around freak waves) and freak waves) in VH and HV polarisation are zero. This result coincides with the well known knowledge about Bragg scattering from the 1D sea surface.

5.2. Backscattering intensity from different pixels of freak waves

We consider the SAR images from freak waves and their background sea waves in Fig. 1 in this section. We truncate the sea surface representation to the domain from –500 m to 500 m at $t = 0$. The wavelength is $\lambda = 200$ m. The whole truncated area is divided into three parts: (a) from –1500 to –500 m, regarded as the area of background sea surface on the left of freak waves, (b) from 500 to 1500 m, which is the area of background sea surface on the other side of the freak waves, and (c) the freak waves area, which is between the two areas.

Figure 6 shows the NRCSs of the freak waves and sine waves for VV polarisation EM waves. It is evident that the NRCSs of freak waves vary approximately with distance in the x-direction in a single period (0.5 times wave length). This result is similar to that of the NRCS for sine waves. Over a period, the largest NRCS occurs separately at crests and troughs in Fig. 1 whereas it is smallest at the average sea level. The NRCSs of freak waves are smaller than those of the sine waves at the same locations. The largest difference in NRCS between the freak waves and the sine waves is –42.7475 dB occurring at the 70 m location in Fig. 3. This result corresponds to the location with a largest steepness between the crests and troughs of the freak waves.

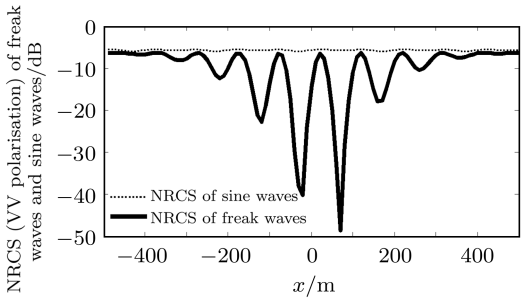


Fig. 6. NRCSs of freak waves and sine waves for VV polarisation EM waves.

In summary, the NRCS of freak waves is smaller than that of the sin waves. From the crests to the troughs of freak waves, the backscatter NRCS varies much faster than that of the normal sine waves. Freak waves also have an extremely low backscatter NRCS at the freak wave facet with the strongest slope.

5.3. Backscattering intensity distribution of incident angles

In order to compare the NRCS of freak waves with that of the background sea surface, we also calculate the NRCSs of freak waves and their background waves (defined in Subsection 5.2). Here the incidence angles vary from 26° to 79° which covers moderate incidence angles, namely the Bragg scattering cases whose incidence angles are in a range of 20°–84°.

Figure 7 shows the backscatter NRCS of background waves with incidence angles varying from 26° to 79°. The NRCS decreases with the increase of incidence angle. Moreover, the NRCS for VV polarisation is larger than that for HH polarisation, which coincides with the well known experimental and numerical results of Kudryavtsev *et al.*[43]

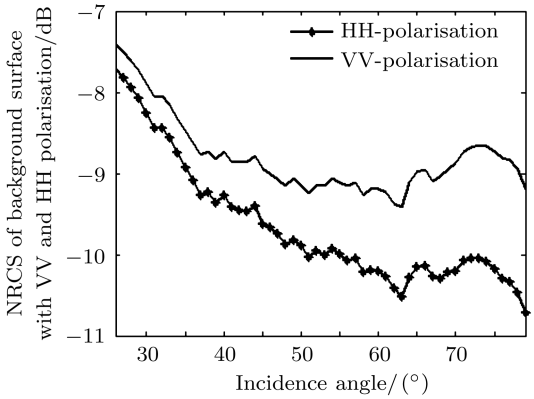


Fig. 7. NRCSs of background sea surface of freak waves in VV and HH polarisations, where incidence angles vary from 26° to 79°.

Comparing the NRCSs for freak waves with those of the background sea surface for VV and HH polarisations (Figs. 8 and 9), one finds that backscatter intensities from freak waves are less than those from the background sea surface for all moderate incidence angles. Therefore, freak waves can be detected for moderate incidence angles suitable for SAR imaging.

Moreover, it is obvious that the variational characteristic for the NRCS at an incidence angle is different from that of background sea surface. NRCS of background sea surface increases with the increase of incident angle when the incidence angle varies from 26° to 79°. However, figure 10 shows a different picture of NRCS variation with incident angle, namely

the NRCSs for freak waves (both HH and VV polarisations) decrease at low incidence angles before reaching their minimum values at a specific incidence angle (denoted as the minimum NRCS value incident angle, MNVI, hereafter), then increase as incident angles increase until reaching their peak NRCS values at another incidence angle. The latter is denoted as the peak NRCS value incidence angle, PNVI, hereafter. The NRCSs of freak waves increase again with the increase of incident angles when incidence angles are larger than the PNVI. In Fig. 10, the MNVI of freak waves in VV polarisation is 46° corresponding to minimum NRCS (–11.63 dB). The PNVI is 72° corresponding to peak NRCS value –9.53 dB. The minimum NRCS of freak waves in HH polarisation is –13.11 dB at MNVI (46°) and the maximum NRCS is –11.5 dB at PNVI (75°).

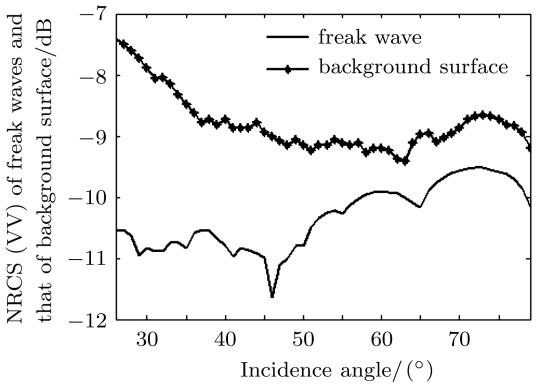


Fig. 8. NRCSs of freak waves and background sea surface for VV polarisation, where incidence angles vary from 26° to 79°.

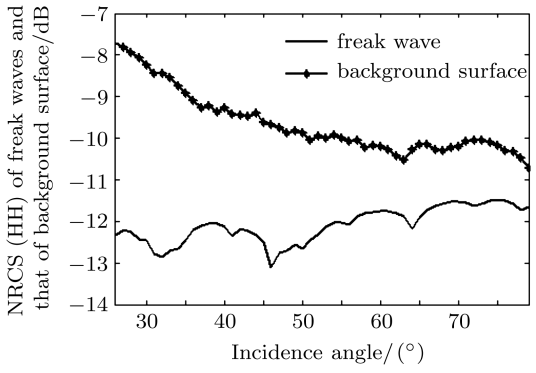


Fig. 9. NRCSs for freak waves and background sea surface for HH polarisation, where incidence angles vary from 26°to 79°.

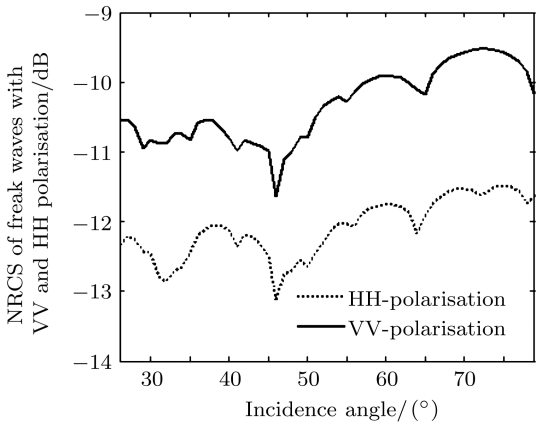


Fig. 10. NRCSs for freak waves for VV and HH polarisations, where incidence angles vary from 26°to 79°.

Figure 11 shows the polarisation ratios between the absolute values of NRCS discrepancy in dB between HH and VV polarisations for the background sea surface and for freak waves. The polarisation ratio of the background sea surface decreases with the increase of incidence angle while the effect of incidence angle on polarisation ratio for freak waves is not notable. Figure 11 shows that the polarisation ratio for freak waves is larger than that of background waves at moderate incidence angles. This implies that echoes backscattered from freak waves are more polarisation-dependent than from the background sea surface in the case of moderate incidence angles.

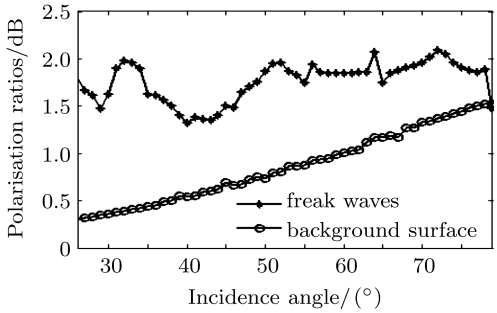


Fig. 11. Polarisation ratio variations with incidence angle for freak waves (asterisk), and for the background sea surface (circle).

These results suggest that the freak waves are easier to detect from the background sea surface with HH polarisation than with VV polarisation. Figure 12 shows that NRCS discrepancies between the freak wave and the background sea surface with HH polarisation are larger than those with VV polarisation when incident angles are less than 79°. The maximum NRCS discrepancy for the HH polarisation echo is 4.615 dB while that of VV polarisation is 3.234 dB, given incidence angles of 26° and 29°, respectively.

The NRCS discrepancies of the HH polarisation echo are almost the same as those of the VV polarisation for large incidence angles (larger than 79°, not shown here). The large ratios for NRCS discrepancies between HH and VV polarisation echoes mainly occur in the incidence angle domains $(26°, 76°)$. Therefore, in SAR images, compared with the case of background sea, the freak waves should be darker in HH polarisation echo images than in VV echo images.

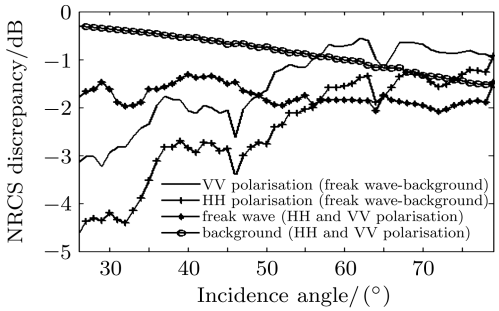


Fig. 12. NRCS discrepancies between freak waves and background sea surface for VV (line) and HH polarisations (plus signs) and ratios of the NRCS discrepancy of HH and VV polarisation echoes for freak wave (asterisk) and background wave(circle).

Finally, one can find that the smaller the incidence angle is, the more easily freak waves in SAR images are detected for both HH and VV polarisations. From Fig. 12, NRCS discrepancies decrease with the increase of incidence angle. For example, the NRCS discrepancy is 1.553 dB in HH polarisation and 0.7155 dB in VV polarisation at incidence angle 60°, whereas it is 4.198 dB in HH polarisation and 2.939 dB in VV polarisation at incidence angle 30°. The image should look like much darker in the freak wave area of the SAR images with 30° incidence angle than with 60° incidence angle. One can infer that smaller incidence angles result in more detectable freak waves in SAR images.

6. Conclusions

Currently, freak waves are not easily detected by remote sensing technology. Therefore, it is necessary to numerically simulate the EM backscattering echoes and study the characteristics of the NRCS of freak waves. Considering the nonlinear interactions between freak waves and Bragg short waves, we present a multiple polarisation EM backscattering model for freak waves. Thus we are able to calculate the NRCSs of freak waves and those of the background sea surface with this model for different cases.

Our numerical results show that the EM backscatter characteristics of freak waves are quite different from those of the normal sea surface (namely the background sea surface). From numerical results, the main differences in EM backscatter characteristic are:

(i) EM backscatter intensities of freak waves are less than those from the background sea surface for all moderate incident angles.

(ii) Echoes backscattered from a freak wave are highly polarisation dependent, even at lower incidence angles. The NRCS of EM backscatter from freak waves has a higher polarisation dependence than that of the background sea surface.

(iii) NRCS discrepancies between freak waves and the background sea surface are larger with HH polarisation than those resulting from VV polarisation, at moderate incident angles.

(iv) NRCS discrepancies between freak waves and the background sea surface decrease as the incidence angle increases, for both HH and VV polarisation, at moderate incident angles.

According to our numerical results, we suggest that freak waves have the extremely low backscatter NRCSs where the freak wave facet has the strongest slope. Freak waves can be detected at moderate incidence angles, which is applicable to SAR imaging. Freak waves can be detected more easily from the background sea surface by HH polarisation than by VV polarisation. Compared with the background sea, freak waves should be darker in HH polarisation echo images than those of VV echo images, in SAR images. The possibility of the detection of freak waves at low incidence angles is much better than freak wave detection at high incidence angles. These results motivate us to further study the detection of freak waves by using SAR images.

References

[1] Draper L 1965 *Mar. Obs.* **35** 193

[2] Dean R G 1990 *Freak Waves: A Possible Explanation, Water Wave Kinematics* (Amsterdam: Kluwer) p609

[3] Kharif C E 2003 *Europe J. Mech.* B: *Fluid* **22** 603

[4] Smith R 1976 *J. Fluid Mech.* **77** 417

[5] Haver S In: Olagnon M and Atanassoulis G (Eds.) 2001

Rogue Waves. p129
[6] Pelinovsky E, Talipova T and Kharif C 2000 *Physics* D **147** 83
[7] Janssen P A E M 2003 *J. Phys. Oceanography* **33** 863
[8] Peterson P, Soomere T, Engelbrecht J and Groesen E 2003 *Nonlinear Progresses in Geophysics* **10** 503
[9] Mori N 2004 *Ocean Engineering* **31** 165
[10] Touboul J, Giovanangeli J P, Kharif C and Pelinovsky E 2006 *J. Eur. J. Mech. B/Fluid* **25** 662
[11] Porubov A V, Tsuji H, Lavrenov I V and Oikawa M 2005 *Wave Motion* **42** 202
[12] Onorato M, Osborne A R and Serio M 2006 *Phys. Rev. Lett.* **96** 14503
[13] Lavrenov I V and Porubov A V 2006 *J. Eur. J. Mech.* B: *Fluid* **25** 574
[14] Petrova P, Cherneva Z and Soares C G 2007 *Ocean Engineering* **34** 956
[15] Fochesato C, Grilli S and Dias F 2007 *Wave Motion* **44** 395
[16] Francesco F 2008 *Physica* D **237** 2127
[17] Janssen P A E M 2008 *J. Comput. Phys.* **227** 3572
[18] Lavrenov L 1998 *Natural Hazards* **17** 117
[19] Yasuda T, Mori N and Ito K 1992 *Proc. of the 23th Int. Conf. on Coastal Eng.* (Venice 1992 ASCE) **1** 751
[20] Yasuda T and Mori N 1994 *International Symposium: Waves-Physical and Numerical Modelling* (Vancouver 1994) **2** 823
[21] Fedele F and Arena F 2005 *Physics of Fluids* **17** 26601
[22] Boccotti P 1983 *Appl. Ocean. Res.* **5** 134
[23] Boccotti P 1997 *Ocean Engineering* **24** 265
[24] Osborne A R, Onorato M, Serio M and Bertone S 2000 *Phys. Lett.* A **275** 386
[25] Schober C M 2005 www.soest.hawaii.edu/PubServices/2005pdfs/Schober.pdf 59
[26] Islas A L and Schober C M 2005 *Physics of Fluids* **17** 31701
[27] Lehner S and Günther H 2004 *Proceeding of IGARSS 04'* **III** 1880
[28] Schulz-Stellenfleth J, Konig T and Lehner S 2007 *J. Geophys. Res.* **112** C03019
[29] Wrighe J 1968 *IEEE Trans. Antennas and Propagation* **16** 217
[30] Holliday D 1987 *IEEE Trans. Antennas and Propagation* **35** 120
[31] Fung A K and Chen K S 1991 *J. Electromagnetic Waves and Applications* **5** 205
[32] Johnson J T, Toporkov J V and Brown G S 2001 *IEEE Trans. Geosci. Remote Sensing* **39** 2411
[33] Xie T, Li B H, Chen W J and He Y J 2004 *Proceeding of IGARSS'04 IV* 2776
[34] Xie T, He Y J, Li B H and Chen W J 2004 *Proceeding of IGARSS'04 IV* 2772
[35] Xie T, He C, William P, Kuang H L, Zou G H and Chen W 2010 *Chin. Phys.* B **19** 024101
[36] Beckmann P and Spizzichino A 1987 *Norwell* (MA: Artech House) p511
[37] Berizzi F and Mese E D 2002 *IEEE Trans. Antennas and Propagation* **50** 426
[38] Plant W J and Keller W C 1990 *J. Geophys. Res.* **95** 16299
[39] Plant W J 2002 *J. Geophys. Res.* **107** 3120
[40] Guo L X and Ren X C 2008 *Chin. Phys.* B **17** 2956
[41] Guo L X and Ren X C 2008 *Chin. Phys.* B **17** 2491
[42] Guo L X, He M X, Wang Y H and Zhang Y M 2008 *Chin. Phys.* B **17** 3696
[43] Kudryavtsev V, Hauser D and Caudal G 2003 *J. Geophys. Res.* **108** 8054
[44] Franceschetti G, Migliaccio M and Riccio D 1998 *IEEE Trans. Geosci Remote Sensing* **36** 84
[45] Dysthe K, Krogstad H E and Müller P 2008 *Annual Review of Fluid Mechanics* **40** 287
[46] Peregrine D H 1983 *J. Australian Math. Soc.* **25** 16
[47] Xie T, Nan C F, Kuang H L, Zou G H and Chen W 2009 *Acta Phys. Sin.* **58** 4011 (in Chinese)
[48] Pan G D and Johnson J T 2006 *IEEE Trans. Geosci. Remote Sensing* **44** 2880
[49] Longuet-Higgins M S and Stewart R W 1960 *J. Fluid Mech.* **8** 565
[50] Xie T, Kuang H L, William P, Zou G H, Nan C F, He C, Shen T and Chen W 2009 *Chin. Phys.* B **18** 3090